https://iopscience.org/ijem

SCIE, EI, SCOPUS, INSPEC, CAS, DOAJ, etc.

International Journal of Extreme Manufacturing

Study of machining indentations over the entire surface of a target ball using the force modulation approach

Yuzhang Wang, Yanquan Geng , Guo Li, Jiqiang Wang, Zhuo Fang and Yongda Yan

Highlights:

- The micro force control principle is proposed to fabricate nanoindentation arrays at different annuli on the whole microsphere surface.
- The key technical issues, such as the alignment of target ball center and the coordinated movement of each axis, are solved during the cutting process of micro-ball surface by using the micro force control principle.
- The influence of processing parameters on the nano-indentations over micro-ball surface under the micro force loading was revealed, and the nanoindentation machining with controllable size over the almost whole surface of target ball was realized.

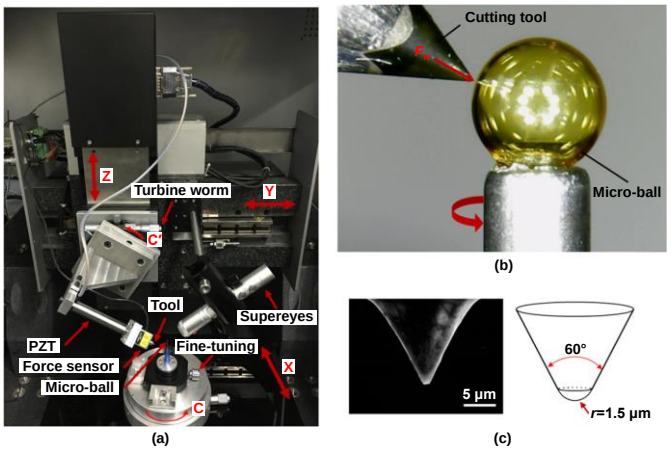

View online: https://iopscience.iop.org/article/10.1088/2631-7990/abff19

Article Download: https://iopscience.iop.org/article/10.1088/2631-7990/abff19/pdf

Citation: Wang Y Z, Geng Y Q, Li G, Wang J Q, Fang Z et al. Study of machining indentations over the entire surface of a target ball using the force modulation approach. *Int. J. Extrem. Manuf.* **3**, 035102(2021).

Related articles:

Towards atomic and close-to-atomic scale manufacturing

Fengzhou Fang, Nan Zhang, Dongming Guo, Kornel Ehmann, Benny Cheung, Kui Liu and Kazuya Yamamura

Citation: Fang F Z, Zhang N, Guo D M, Ehmann K, Cheung B et al. Towards atomic and close-to-atomic scale manufacturing. *Int. J. Extrem. Manuf.* **1**, 012001 (2019).

Manufacturing technologies toward extreme precision

Zhiyu Zhang, Jiwang Yan and Tsunemoto Kuriyagawa

Citation: Zhang Z Y, Yan J W, Kuriyagawa T. Manufacturing technologies toward extreme precision. *Int. J. Extrem. Manuf.* **1**, 022001 (2019).

Dynamic modeling of ultraprecision fly cutting machine tool and the effect of ambient vibration on its tool tip response

Jianguo Ding, Yu Chang, Peng Chen, Hui Zhuang, Yuanyuan Ding, Hanjing Lu and Yiheng Chen

Citation: Ding J G, Chang Y, Chen P, Zhuang H, Ding Y Y et al. Dynamic modeling of ultra-precision fly cutting machine tool and the effect of ambient vibration on its tool tip response. *Int. J. Extrem. Manuf.* **2**, 025301 (2020).

OPEN ACCESS
IOP Publishing | IMMT
International Journal of Extreme Manufacturing
Int. J. Extrem. Manuf. **3** (2021) 035102 (9pp)
https://doi.org/10.1088/2631-7990/abff19

Study of machining indentations over the entire surface of a target ball using the force modulation approach

Yuzhang Wang[1,2], Yanquan Geng[1,2], Guo Li[3], Jiqiang Wang[1,2], Zhuo Fang[1,2] and Yongda Yan[1,2,*]

[1] Key Laboratory of Micro-systems and Micro-structures Manufacturing of Ministry of Education, Harbin Institute of Technology, Harbin, Heilongjiang 150001, People's Republic of China
[2] Center for Precision Engineering, Harbin Institute of Technology, Harbin, Heilongjiang 150001, People's Republic of China
[3] Research Center of Laser Fusion, China Academy of Engineering Physics, Mianyang, Sichuan 621900, People's Republic of China

E-mail: yanyongda@hit.edu.cn

Received 8 November 2020, revised 10 February 2021
Accepted for publication 7 May 2021
Published 21 May 2021

Abstract

A modified five-axis cutting system using a force control cutting strategy was to machine indentations in different annuli on the entire surface of a target ball. The relationship between the cutting depths and the applied load as well as the microsphere rotation speed were studied experimentally to reveal the micromachining mechanism. In particular, aligning the rotating center of the high precision spindle with the microsphere center is essential for guaranteeing the machining accuracy of indentations. The distance between adjacent indentations on the same annulus and the vertical distance between adjacent annuli were determined by the rotating speed of the micro-ball and the controllable movement of the high-precision stage, respectively. In order to verify the feasibility and effect of the proposed cutting strategy, indentations with constant and expected depths were conducted on the entire surface of a hollow thin-walled micro-ball with a diameter of 1 mm. The results imply that this machining methodology has the potential to provide the target ball with desired modulated defects for simulating the inertial confinement fusion implosion experiment.

Keywords: force modulation, controllable indentations, entire micro-ball surface, microsphere center alignment

1. Introduction

A normal inertial confinement fusion (ICF) implosion continuously compresses an imploding outer spherical shell towards the target ball center by an intense radiation field, incessantly condensing and heating the fission fuel within the shell until meeting fire requirements [1–3]. Due to the inherent defects in the target surface, the asymmetric compression will trigger implosion in the weak part, which can break the target surface or result in performance failure from the generated Rayleigh–Taylor (RT) instability on the surface of the fuel-shell [4, 5]. Thus, RT instability has been a critical research field with considerable experiments and intensive theories due to its influence on ICF behaviors [6, 7]. The defects and roughness of the target surface have been found to strongly affect RT instability [8–10]. The shapes and sizes of target defects are various and randomly distributed. In order to investigate the

* Author to whom any correspondence should be addressed.

2631-7990/21/035102+9$33.00

formation circumstances of RT instability, there is no doubt that it is an urgent need to fabricate nanostructures with modulated and controllable dimensions, which can simulate defects on a target surface, so as to analyze the ICF experiments. Most explorations regarding this subject focus on flat targets, where the evolution somewhat differs from a converging geometry [11–13]. For example, a hollow thin-walled microsphere around 1 mm in diameter is always regarded as a target ball. However, no effective processing technique exists for solving the issue of easy deformation when machining nanostructures on the surface of low-stiffness micro-balls. Therefore, fabricating high-precision nanostructures on the whole surface of a microsphere remains a challenge.

Nowadays, several processing approaches, such as laser fabrication [14–16], micro turning [17–19], nanomachining based on atomic force microscope (AFM) [20–22] and fast tool servo (FTS) [23–25] cutting, have been adopted to prepare nanostructures on microsphere surfaces. In 2000, some scholars prepared a template of microstructures by excimer laser processing. They obtained a sinusoidal microstructure with a period of 60 μm and amplitude of 1 μm through imprinting on a 280 μm $\times$ 280 μm area of the micro-ball surface [11]. However, due to the localization of the machining area and the complexity of the polymer processing mechanism, this method is restricted in the application of fabricating microstructures on an entire rotary surface. Microgrooves with an average width of 30 μm and a depth of 30 μm depth were achieved on the microsphere surface by utilizing a six-axis ultra-precision machining center [26]. Although the machining accuracy and the sizes of machined structures can reach the micron level using diamond micro turning, it is difficult to accurately control the expected depths at the nanoscale because of the motion and limited detection precision of the machine tool. The AFM tip-based nanomechanical machining technique [27, 28], in which the cutting tip applies constant normal forces to the sample, can fabricate nanodots [29, 30], nanowires [31, 32], nanochannels [33, 34], and square-shaped, circular, and triangular cavities on the microsphere surface [35]. Despite the fact that the AFM nanomachining approach is regarded as an effective method to machine microstructures on curved surfaces [36–38], the prominent disadvantages are its low efficiency with a machining speed below 1 mm min^{-1}, serious tool wear, simple nanostructures, and most importantly limited machining area as well as small depths with approximate 200 nm [39]. For the sake of solving the difficulties in machining large depths over the non-planar surfaces of hard-brittle materials, the force control FTS has been developed by learning from the AFM-based cutting strategy as well as the rigid body of the machine tool for realizing high precision and high efficiency fabrication. Differing from AFM tip-based nanomachining, the force control FTS supports sufficient stiffness and much longer servo motion for the purpose of machining large depths over large areas [40].

This paper proposes a novel approach using force modulation between cutting tool and workpiece to fabricate nanostructures with relatively large machined depths at different annuli on the whole surface of a brittle material target ball, which breaks through the traditional rigid principle of tool-based diamond cutting by displacement control. A distinct advantage of the proposed force modulation cutting strategy is similar to AFM-based nanomachining, in which a force sensor measures the normal force loaded onto the micro-ball, and a desired normal force can be loaded onto the cutting tip by controlling the displacement of PZT. As a result, nanostructures with consistent depths can be achieved by keeping the normal forces constant during scratching. Thus, with regard to the employed force modulation cutting method in this study, the sensitivity or measurement accuracy of the force sensor as well as the material removal state mainly contributes to the machining accuracy, and the stiffness of this system has no influence on the form accuracy of indentations. This paper is presented in the following sections. Section 2 briefly describes the establishment of a five-axis micromachining experimental setup based on a force feedback control system. In addition, the relationship between the normal forces and machined depths of the indentations as well as the processing technique, such as the alignment of the microsphere center, are analyzed.

2. Experimental details

2.1. Experimental setup

The modified five-axis micromachining system using load modulation is shown in figure 1(a). This machining system is composed of air floatation-driven high precision stages (X) and (Y) with a resolution and stroke of 100 mm and 1 nm, respectively, as well as a motor-driven coarse stage (Z) with a resolution of 0.5 μm. These stages were used to adjust the position of the cone tip relative to the micro-ball. Figure 1(c) reveals the scanning electron microscopy (SEM) images and the geometry of the conical diamond cone tip, which was employed in the indentation process. AFM scanning estimated that the cone angle was 60° and the arc radii (r) of cone tip was 1 μm. During the machining process, the rotating speed of the micro-ball was precisely controlled by an air-bearing rotary stage (C), with a radial rotation accuracy of 0.26 μm, to control the distances between adjacent indentations. A fine-tuning stage (LA1V-XY, NEWPORT Corporation, USA) with a dimensional resolution of 0.75 μm was fixed on the rotary platform to align the microsphere center with the rotating center and prevent low form accuracy from a serious eccentric error. During the indentation process, the cutting tip was aimed at the micro-ball center by a turbine worm rotating platform (OptoSigma Corporation, KSPA-986M, Japan), which has a rotating range and resolution of 360° and 52.9″, respectively. The force-feedback control system also contains essential components, including a controller (UMAC, Delta Tau Data Systems, Los Angeles, CA, USA), a piezoelectric (PZT) actuator (PSt150/7/60VS12, COREMORROW, Harbin, China), and a force sensor of 50 g capacity (LSB-200, FUTEK, Irvine, CA, USA).

In this study, a hollow thin-walled polymer microsphere with a diameter and wall thickness of 1 mm and 30 μm, respectively, as shown in figure 1(b), was glued to a syringe needle. Both the applied force and the rotation speed of spindle

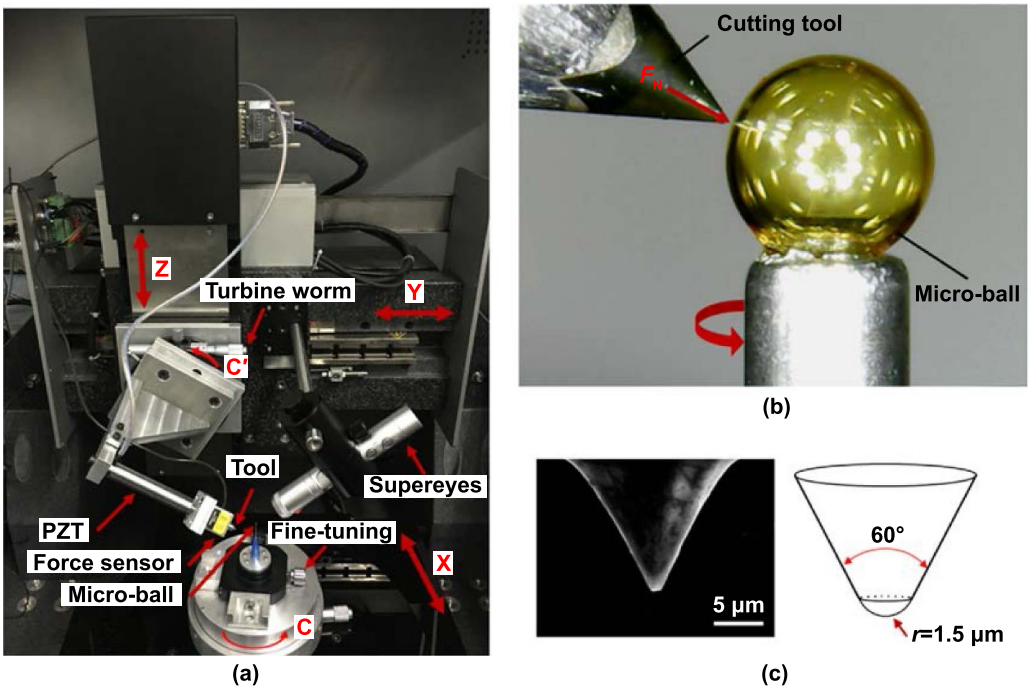

Figure 1. (a) Photograph of the experimental setup. (b) Optical image of the micro-ball and cutting tool. (c) SEM images and geometry of the diamond cone tip.

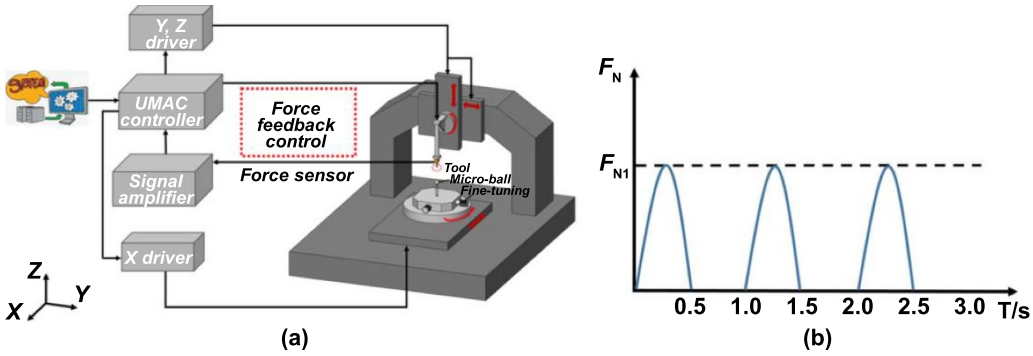

Figure 2. (a) Schematic of the proposed machining system and (b) periodic sinusoidal reference signal of applied normal force.

in the indentation process remained constant. The topography of the machined indentations was observed through the tapping mode of AFM (Dimension Icon; Bruker Corporation, USA) using a silicon tip (TESPA, Bruker Company, USA) with a resonant frequency of 13 kHz and spring constant of 0.2 N m^{-1}.

2.2. Methodology of indenting on the microsphere surface

Figure 2(a) reveals the schematic of the proposed machining principle for the force feedback control system. The normal force loaded on the surface of the micro-ball through the tool tip was measured by a high-sensitivity force sensor. Depending on the loaded normal force (F_N) and the reference signal of the periodic sinusoidal force, the UMAC controller decides to extend or retract the PZT actuator to reach the feedback control requirements. Figure 2(b) indicates that the period of applied normal force was set at 1 s. During the first 0.5 s, the normal force was loaded from zero to the expected peak and then unloaded to zero. Afterwards, the normal force was kept at zero for an additional 0.5 s. Moreover, when the rotating speed of micro-ball was fixed, the shorter the period of normal force, the more indentations achieved. Although the computer program can adjust the period of normal force, the limited response frequencies of PZT and the force sensor as well as crowded indentations on one annulus, significantly influence the form accuracy of the machined indentations.

In order to obtain consistent indentations on the same annulus of the microsphere during the continuous indentation process, the micro-ball rotated at a constant angular speed, and the cutting tool carried out reciprocating motions via the PZT actuator, ensuring the constant depth of each indentation. Obviously, the value of sinusoidal force amplitude determines the cutting depths of indentations. The angular speed of the micro-ball rotation determined both the number of indentations on the same annulus and the distance between adjacent

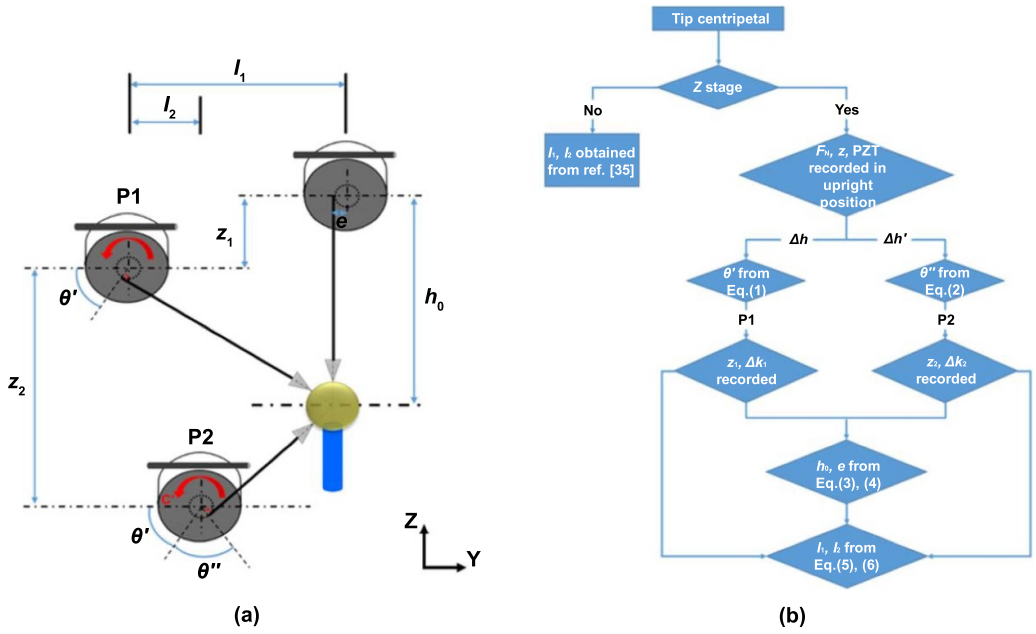

Figure 3. (a) Schematic of the relationship between the rotation angle of the diamond cone tip and moving distances in *Y* and *Z* directions and (b) illustration of calculation process.

indentations. In addition, the distance between different annuli was adjusted by a high precision moving stage Y and a coarse moving stage Z as well as a turbine worm rotating platform, which is described in the following section 2.4.

2.3. Alignment of the micro-ball center

If the cone tip coincides with the center of the microsphere during the whole indentation process, it guarantees the consistency of each indentation and the same distance between adjacent indentations, while considering the PZT's limited range of motion. Therefore, aligning the microsphere center with the rotating center of the air-bearing driven high precision spindle is absolutely essential. Firstly, for the coarse alignment, the 2D fine-tuning stage with the glued microsphere was installed on the rotary platform, which rotated a microsphere 360°. Optical capture software monitored the microsphere's center position. For the fine alignment process, the 2D fine-tuning stage was used to adjust the position of the micro-ball. The details of the centering adjustment method are provided below.

(a) The high-precision spindle stays stationary at position 1. Meanwhile, the circular features, including the spherical center position and contour of the microsphere, can be obtained by extracting eight points uniformly distributed on the dynamic video capture projection image.
(b) The microsphere rotates 180° to position 2. Using a method similar to step 1, another circular contour can be obtained. An optical software conducts the centering adjustment operation.
(c) By fitting the two rotation centers and contours of the microspheres obtained in steps 1 and 2 to be completely coincident, the rotation center and contour of the microsphere should be the position where the microsphere center coincides with the spindle gyration center.
(d) The microsphere is moved to the new circular contour along the orthogonal directions of the 2D manual fine-tuning stage through two screws that adjust the position.
(e) The high-precision spindle rotates 180° to verify that the center of microsphere coincides with the spindle gyration center by observing the circular contour. If the position of the micro-ball is always within this circular contour, the process of fine centering alignment is successfully completed. Otherwise, the above steps should be repeated.

2.4. Movement calculation for indenting on different annuli

For machining indentations at different annuli, the cone tip was rotated along the entire surface of the microsphere by a turbine worm rotating platform. However, it is difficult to make the cone tip coincide with the microsphere center when moving from one annulus to another, which results in the failure of geometries of machined indentations. Stated in the previous study [35], the largest rotation angle of the cutting tool is restricted by the moving capacity of the 2D high precision stage. With the improvement of micromachining tools, any desired rotation angle of the cutting tool can be implemented by the high-precision stages Y and Z and the turbine worm rotating platform in this study. The principle of accurate mathematic calculation for the relationship between the rotation angle (θ) of the cone tip and moving distances in *Y* and *Z* directions is illustrated in figure 3(b).

Firstly, note that a vertical distance inevitably exists between the cutting tip and the rotating center of the turbine worm stage, defined as *e* in figure 3(a). In the upright direction of PZT, the cutting tool applies very little force when approaching the microsphere vertex. In the meantime, the

current position of PZT is recorded. For machining on the first annulus, the cone tip was lifted and the required rotation angle (θ') was developed by the chosen vertical distance between the vertex of the microsphere and the desired machined annulus (Δh), as follows:

$$\Delta h = R - R\cos\theta' \tag{1}$$

where R is the radius of the microsphere. Based on the rotating angle (θ'), the Y and Z stages move over distances l_1 and z_1, respectively. When machining on the first annulus, the same normal force was loaded for approaching the surface of the microsphere and recording the extension value of PZT. Compared with the value recorded in the upright position of PZT, the increasing value of PZT extension (Δk_1) can be calculated. When indenting on the second annulus, the cone tip was adjusted to continue rotating another angle (θ'') depending on the desired vertical distance ($\Delta h'$) between the first machined annuli and second one, as solved in the following equation:

$$\Delta h' = R\cos\theta' + R\cos\left(180^\circ - (\theta' + \theta'')\right). \tag{2}$$

The previously mentioned steps were repeated, including moving a distance of l_2 and z_2, obtaining the difference (Δk_2) between the upright position of PZT in the case of rotating θ''. Thus, the value of h_0 and e can be derived in the form of:

$$h_0 - z_1 = \cos\theta'(h_0 + \Delta k_1 + e\tan\theta') \tag{3}$$

$$\begin{aligned} z_1 + z_2 - h_0 = {} & \sin\left((\theta' + \theta'') - 90^\circ\right)[h_0 + \Delta k_2 \\ & - e\tan\left(180^\circ - (\theta' + \theta'')\right)] \end{aligned} \tag{4}$$

where θ', θ'', z_1, z_2, Δk_1, and Δk_2 are known parameters. The moving distances l_1 and l_2 of the high-precision stage Y defined with respect to the tip rotating angles of θ' and θ'', respectively, are described by the following equations (5) and (6), which consider the geometry relationship as shown in figure 3(a):

$$l_1 = (h_0 - z_1)\tan\theta' - \frac{e}{\cos\theta'} + e \tag{5}$$

$$\begin{aligned} l_1 - l_2 = {} & (z_1 + z_2 - h_0)\tan\left(180^\circ - (\theta' + \theta'')\right) \\ & + \frac{e}{\cos\left(180^\circ - (\theta' + \theta'')\right)} + e. \end{aligned} \tag{6}$$

3. Results and discussion

3.1. Fabrication by loading different normal forces

To evaluate the capability of the proposed five-axis micromachining system using a force modulation cutting strategy, the experiments of indenting by varying the loading normal forces were first conducted on the microsphere surface. The amplitudes of applied normal forces were set at 5, 10, 15, 17, 20, 23, 26, and 30 mN. And the rotation speed of the spindle was held constant at $3^\circ s^{-1}$.

The AFM images with cross section measurements corresponding to the setting normal forces of 5, 10, 17, 23, and 30 mN are shown in figure 4. The indentation depths were evaluated to be 0.83, 1.2, 3.14, 3.58, and 4.01 μm. The relationship between the applied normal forces and cutting depths is illustrated in figure 6(a). Three regions of the map were clearly observed. In the case of machining forces from 5 to 15 mN, when the indenting depth was smaller than the arc radius of cone tip, approximately 1.5 μm, the spherical cap of the cutting tool played a critical role in machining. However, as the applied normal forces increased to the second part from 15 mN to the critical point of 17 mN, the indentation depths increased dramatically from 1.58 μm to 3.14 μm. This phenomenon occurred because the machined depths were significantly larger than the arc radii of the cone tip. As a result, the spherical cap and the cutting edge participated in the indentation process, which dramatically increased the machining depths. For the third part with cutting forces larger than 17 mN, the growth rate of the depths slowed. This might be attributed to the influence of material pile-up. The tool edges contributed more to the indentation depths.

3.2. Fabrication by varying the rotating speed of the micro-ball

To identify the influence of the microsphere's rotating speed on the topography of the machined indentations, the experiments were extended to make indentations by selecting rotating speeds from $1^\circ s^{-1}$ to $3^\circ s^{-1}$ with an increment of $0.5^\circ s^{-1}$. The applied normal force was set at 10 mN.

The AFM images and the section profiles corresponding to rotating speeds of $1^\circ s^{-1}$, $2^\circ s^{-1}$, and $3^\circ s^{-1}$ are presented in figure 5. The depths were consistent and evaluated to be 1.4, 1.21 and 1.21 μm. As shown in figure 6(b), the rotating speed of the microsphere within a certain range, that is, increasing from $1^\circ s^{-1}$ to $3^\circ s^{-1}$, has little influence on the depths of the machined indentations. The depths obtained from rotating speeds less than $1.5^\circ s^{-1}$ were almost unchanged. When the rotating speed increased to $2^\circ s^{-1}$, the machined depth obtained was slightly smaller. As the rotating speed increased to $3^\circ s^{-1}$, the depths became constant again. More importantly, it is evident from figure 7 that the shape of machined indentations differed from the shape of the cone tip, which suggests that the machined indentations tailed off in the direction opposite of the micro-ball rotation. This was mainly attributed to the fact that the micro-ball remained rotating during the entire loading and unloading process of tracking the sinusoidal normal force signal. That is to say, when the machining tip contacted the micro-ball surface, the microsphere kept moving. Furthermore, the faster the rotating speed of microsphere, the larger the tailing off of the machined indentations. That is the reason why the rotating speed should be controlled within $3^\circ s^{-1}$ to avoid unexpected nanostructures. In addition, the microsphere was made of a hard, brittle polymer. Thus, slight deformation or squeezing might occur during the material removal process. When the cutting tip left from the surface of the micro-ball, the material elastic recovery contributed to minor shape deviation.

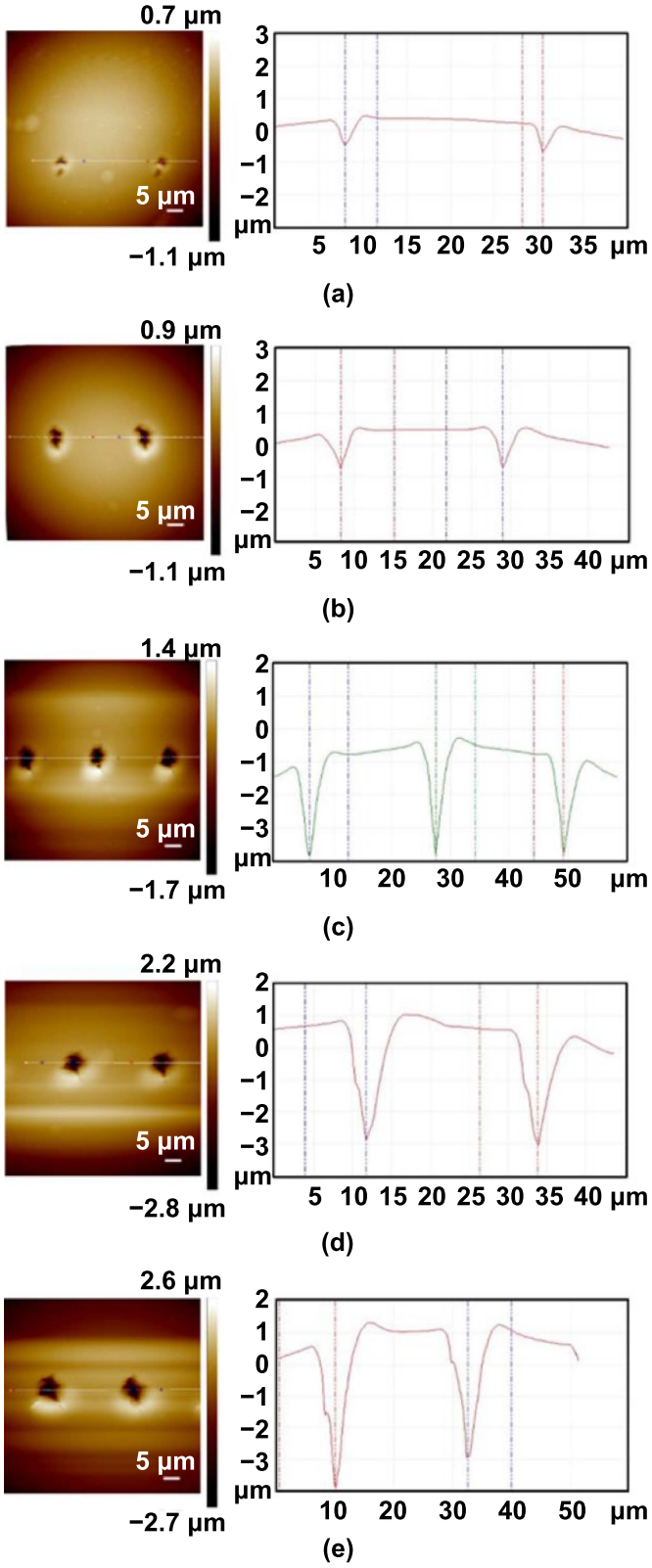

Figure 4. AFM images of the machined indentations: (a) 5 mN, (b) 10 mN, (c) 17 mN, (d) 23 mN, and (e) 30 mN.

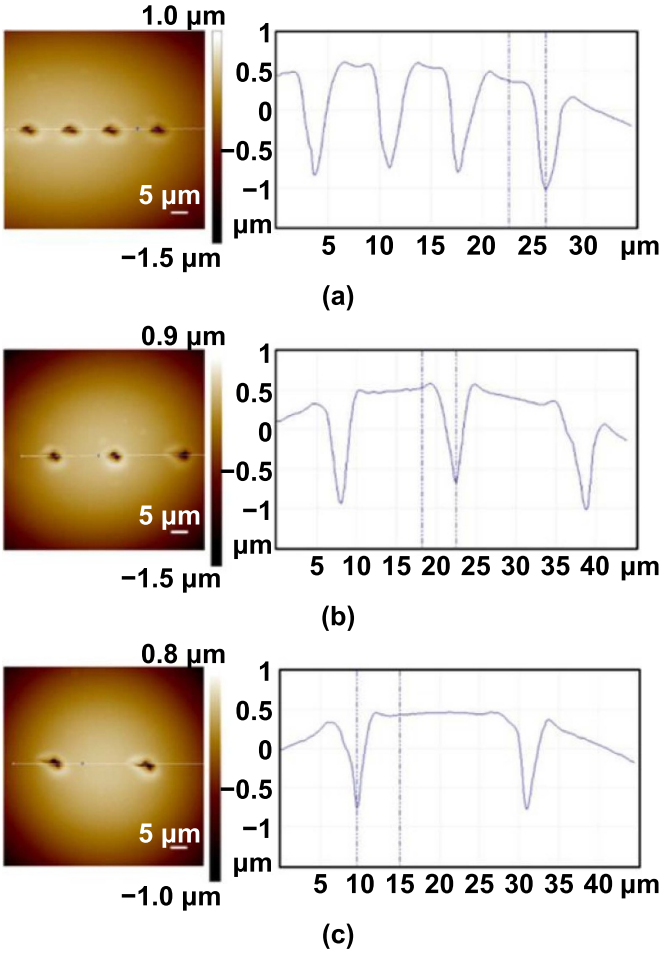

Figure 5. AFM images of machined indentations by 10 mN: (a) $1^{\circ}s^{-1}$, (b) $2^{\circ}s^{-1}$, and (c) $3^{\circ}s^{-1}$.

3.3. Fabrication of indentations on the entire surface of a microsphere

In order to demonstrate the effectiveness of machining nanostructures over the entire microsphere surface using the proposed five-axis micromachining system, the indentations were conducted on different annuli of the micro-ball. Since the annuli on the microsphere have different radii, the circumferences of the annuli are different. However, the computer program ensured that the same number of indentations were made on each annulus. Therefore, the selected rotating speed should not be too slow, as to avoid the overlapping of adjacent indentations on the annulus with a smaller circumference due to the dense indentation. At the same time, considering the surface quality of the machined indentations, the rotating speed should not be too fast to cause tailing. To this end, the rotating speed was set at $2^{\circ}s^{-1}$, that is, there were 180 indentations on each annulus, and the machining time took 180 s. According to the relationship between the normal forces and machining depths,

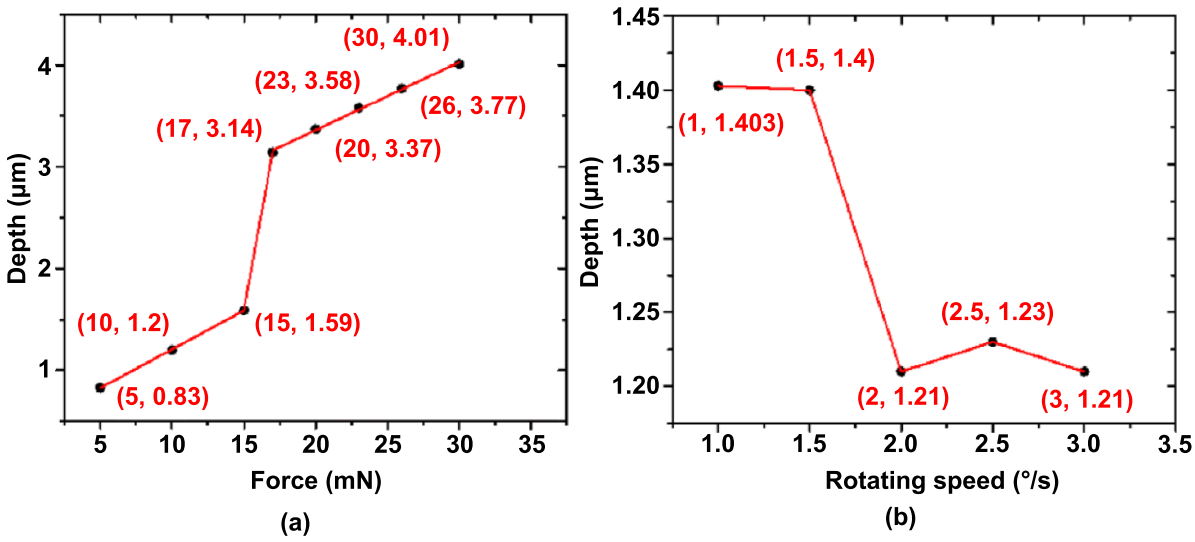

Figure 6. Relationship between the indentation depths and (a) the applied forces and (b) the microsphere rotating speed.

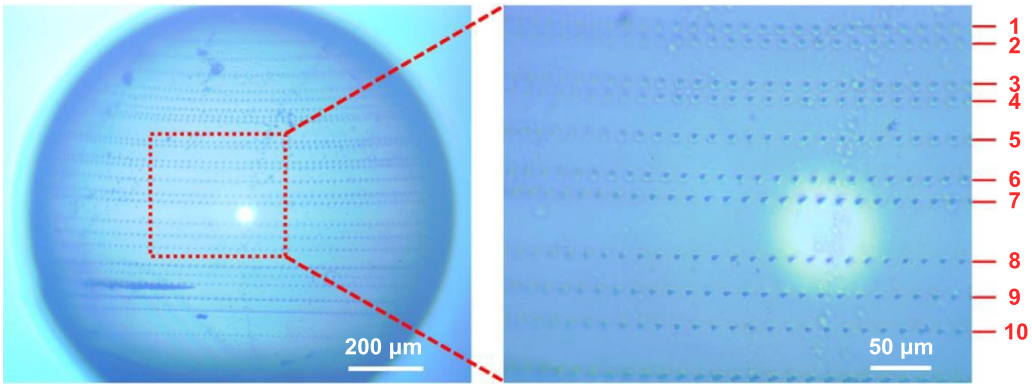

Figure 7. Entire and local optical images of the machined indentations over the whole microsphere surface.

as shown in figure 6(a), the amplitude of normal force was set at 10 mN to prevent puncturing the hollow thin-walled micro-ball. In the present study, 28 different annuli located on the entire surface of microsphere were selected for the indentation process. The vertical distance between adjacent annuli and the high precision stage movement were calculated by applying the method described in section 2.4.

As shown in figure 7, the overall optical image of the obtained indentations over the entire microsphere surface and the local image of the indentations on different annuli are marked from '1' to '10.' The following controllable vertical distances between adjacent annuli were achieved: 12 μm between '1' and '2', '3' and '4'; 32 μm for '4' and '5', '5' and '6'; 28 μm for '8' and '9', '9' and '10'. Cross-sections of two different positions were obtained by AFM scanning to assess the quality of indentations over the whole microsphere's surface (i.e. depth and consistency). There is no doubt that the indentation cutting depths were guaranteed to be constant at positions 1 and 2, where the depths were 1.4 μm and 2.1 μm, respectively, as indicated in figure 8. However, notice that the depths in both positions were different. A possible reason for this was that the surface material of micro-ball had a considerable effect on the machined depths, which means that the microsphere material was not uniform. In the future, according to the indentation depths, the distribution of material on the surface of the microsphere may be preliminarily judged by selecting processing indentations at different positions on the entire surface of the microsphere. The goal of machining indentations at different annuli over the entire microsphere surface using the proposed cutting strategy was achieved.

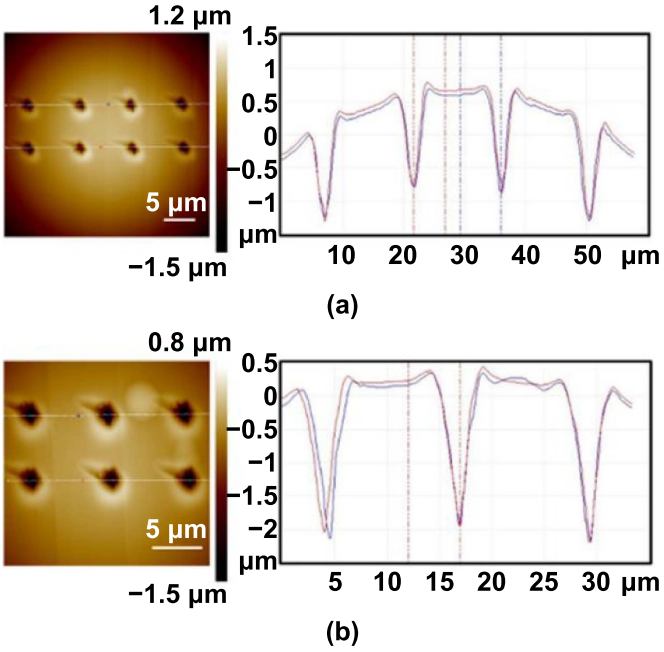

Figure 8. AFM images of machined indentations by 10 mN and rotating speed of $2^{\circ}s^{-1}$: (a) position 1 and (b) position 2.

4. Conclusions

This paper investigated the possibility of machining indentations at different annuli over a hollow thin-wall microsphere surface with a 1 mm diameter using the proposed tip-based micromachining approach. The influence of loaded normal forces and micro-ball rotating speeds on the machined indentation depths were explored. The rotating speed of the micro-ball determines the distance between adjacent indentations on the same. Based on the movement calculation, adjusting the high precision stage and the worm rotating platform based on the movement calculation can control the vertical distance between adjacent annuli. Most importantly, the microsphere center should be aligned with the gyration center of rotating stage, which is a key factor to ensuring the surface quality of machined indentations. Finally, the effectiveness of the proposed methodology of machining nanostructures on the entire surface of microsphere was validated successfully. Furthermore, these positive results are expected to overcome the difficulties of machining high precision 3D nanostructures on the target ball surfaces used in ICF experiments, which will promote the improvement of RT instability research.

Acknowledgments

The authors gratefully acknowledge the financial support of the National Natural Science Foundation of China (52035004, 21827802), Natural Science Foundation of Heilongjiang Province of China (YQ2020E015), Self-Planned Task (No. SKLRS202001C) of State Key Laboratory of Robotics and System (HIT), and 'Youth Talent Support Project' of the Chinese Association for Science and Technology.

ORCID iD

Yanquan Geng https://orcid.org/0000-0003-3499-0551

References

[1] Sadot O, Smalyuk V A, Delettrez J A, Meyerhofer D D, Sangster T C, Betti R, Goncharov V N and Shvarts D 2015 Observation of self-similar behavior of the 3D, nonlinear Rayleigh–Taylor instability *Phys. Rev. Lett.* **95** 265001

[2] Mehlhorn T A *et al* 2003 Recent experimental results on ICF target implosions by Z-pinch radiation sources and their relevance to ICF ignition studies *Plasma Phys. Control. Fusion* **45** A325

[3] Weber C, Ali S, Biener J, Celliers P M, Clark D and Haan S W 2018 Simulations of the impact of ablator micro-structure on ICF implosions *Proc. 60th Annual Meeting of the APS Division of Plasma Physics* (Portland, OR: Bulletin of the American Physical Society)

[4] Lindl J 1995 Development of the indirect-drive approach to inertial confinement fusion and the target physics basis for ignition and gain *Phys. Plasmas* **2** 3933–4024

[5] Giraldez E M *et al* 2016 Machining of Two-dimensional sinusoidal defects on ignition-type capsules to study hydrodynamic instability at the national ignition facility *Fusion Sci. Technol.* **70** 258–64

[6] Remington B A *et al* 1997 Supernova hydrodynamics experiments on the Nova laser *Phys. Plasmas* **4** 1994–2003

[7] Casner A *et al* 2013 Design and implementation plan for indirect-drive highly nonlinear ablative Rayleigh–Taylor instability experiments on the National Ignition Facility *High Energy Density Phys.* **9** 32–7

[8] Sinars D B *et al* 2013 The effect of surface roughness and structure on subsequent magneto-Rayleigh-Taylor instability growth in beryllium liner implosions on Z *2013 Abstracts IEEE Int. Conf. on Plasma Science* (San Francisco, CA: IEEE)

[9] Awati V B, Chavaraddi K B and Gouder P M 2019 Effect of boundary roughness on nonlinear saturation of Rayleigh-Taylor instability in couple-stress fluid *Nonlinear Eng.* **8** 39–45

[10] Pullin D I 1982 Numerical studies of surface-tension effects in nonlinear Kelvin–Helmholtz and Rayleigh–Taylor instability *J. Fluid Mech.* **119** 507–32

[11] Glendinning S G *et al* 2000 Ablation front Rayleigh–Taylor growth experiments in spherically convergent geometry *Phys. Plasmas* **7** 2033–9

[12] Bates J W, Schmitt A J, Karasik M and Zalesak S T 2016 Numerical simulations of the ablative Rayleigh-Taylor instability in planar inertial-confinement-fusion targets using the FastRad3D code *Phys. Plasmas* **23** 122701

[13] Zhao K G, Xue C, Wang L F, Ye W H, Wu J F, Ding Y K, Zhang W Y and He X T 2019 Two-dimensional thin shell model for the nonlinear Rayleigh-Taylor instability in spherical geometry *Phys. Plasmas* **26** 022710

[14] Guo B S, Sun J Y, Hua Y H, Zhan N W, Jia J G and Chu K P 2020 Femtosecond laser micro/nano-manufacturing: theories, measurements, methods, and applications *Nanomanuf. Metrol.* **3** 26–67

[15] Lundgren E H and Forsman A C 2009 Laser forming of shaped fill holes in beryllium targets for inertial confinement fusion experiments *Fusion Sci. Technol.* **55** 325–30

[16] Smalyuk V A, Sadot O, Delettrez J A, Meyerhofer D D, Regan S P and Sangster T C 2005 Fourier-space nonlinear Rayleigh-Taylor growth measurements of 3D laser-imprinted modulations in planar targets *Phys. Rev. Lett.* **95** 215001

[17] Rahman M A, Rahman M, Kumar A S and Lim H S 2005 CNC microturning: an application to miniaturization *Int. J. Mach. Tools Manuf.* **45** 631–9
[18] Wu B Q, Sun Y J, Leng Y B, Li W and Dong L H 2015 Research on the fabrication of the curved surface micro-lens for the laser safety *2015 Int. Conf. on Optoelectronics and Microelectronics (ICOM)* (Changchun: IEEE)
[19] Ito S, Iijima D, Hayashi A, Aoyama H and Yamanaka M 2002 Micro turning system: a super small CNC precision lathe for microfactories *J. Japan Soc. Grinding Eng.* **46** 330–3
[20] Mathew P T, Rodriguez B J and Fang F Z 2020 Atomic and close-to-atomic scale manufacturing: a review on atomic layer removal methods using atomic force microscopy *Nanomanuf. Metrol.* **3** 167–86
[21] Fang T H and Chang W J 2003 Effects of AFM-based nanomachining process on aluminum surface *J. Phys. Chem. Solids* **64** 913–8
[22] Lin H Y, Chen H A, Wu Y J, Huang J H and Lin H N 2010 Fabrication of metal nanostructures by atomic force microscopy nanomachining and related applications *J. Nanosci. Nanotechnol.* **10** 4482–5
[23] Zhang H J, Chen S J, Zhou M and Yang Y H 2009 Fast tool servo control for diamond-cutting microstructured optical components *J. Vac. Sci. Technol.* B **27** 1226–9
[24] Zhou M, Zhang H J and Chen S J 2010 Study on diamond cutting of nonrationally symmetric microstructured surfaces with fast tool servo *Mater. Manuf. Process.* **25** 488–94
[25] Lu H, Lee D, Kim J and Kim S 2014 Modeling and machining evaluation of microstructure fabrication by fast tool servo-based diamond machining *Precis. Eng.* **38** 212–6
[26] Takeuchi Y, Yoneyama Y, Ishida T and Kawai T 2009 6-Axis control ultraprecision microgrooving on sculptured surfaces with non-rotational cutting tool *CIRP Ann.* **58** 53–6
[27] Tseng A A 2011 Removing material using atomic force microscopy with single- and multiple-tip sources *Small* **7** 3409–27
[28] Yan Y D, Geng T Q and Hu Z J 2015 Recent advances in AFM tip-based nanomechanical machining *Int. J. Mach. Tools Manuf.* **99** 1–18
[29] Kawasegi N, Takano N, Oka D, Morita Y, Shigeru Y, Kanda K, Takano S, Obata T and Ashida K 2006 Nanomachining of silicon surface using atomic force microscope with diamond tip *J. Manuf. Sci. Eng.* **128** 723–9
[30] Kobayashi T and Yan J W 2020 Generating nanodot structures on stainless-steel surfaces by cross scanning of a picosecond pulsed laser *Nanomanuf. Metrol.* **3** 105–11
[31] Zhao X S, Geng Y Q, Li W B, Yan Y D, Hu Z J, Sun T, Liang Y C and Dong S 2012 Fabrication and measurement of nanostructures on the micro ball surface using a modified atomic force microscope *Rev. Sci. Instrum.* **83** 115104
[32] Elkaseer A and Brousseau E B 2014 Modelling the surface generation process during AFM probe-based machining: simulation and experimental validation *Surf. Topogr.* **2** 025001
[33] Geng Y Q, Yan Y D, Zhao X S, Hu Z J, Liang Y C, Sun T and Dong S 2013 Fabrication of millimeter scale nanochannels using the AFM tip-based nanomachining method *Appl. Surf. Sci.* **266** 386–94
[34] Yan Y D, Geng Y Q, Hu Z J, Zhao X S, Yu B W and Zhang Q 2014 Fabrication of nanochannels with ladder nanostructure at the bottom using AFM nanoscratching method *Nanoscale Res. Lett.* **9** 212
[35] Geng Y Q, Wang Y Z, Yan Y D and Zhao X S 2017 A novel AFM-based 5-axis nanoscale machine tool for fabrication of nanostructures on a micro ball *Rev. Sci. Instrum.* **88** 115109
[36] Park S S, Mostofa M G, Park C I, Mehrpouya M and Kim S 2014 Vibration assisted nano mechanical machining using AFM probe *CIRP Ann.* **63** 537–40
[37] Napolitano S, D'Acunto M, Baschieri P, Gnecco E and Pingue P 2012 Ordered rippling of polymer surfaces by nanolithography: influence of scan pattern and boundary effects *Nanotechnology* **23** 475301
[38] Brousseau E, Al-Musawi R S J and Lebiez D 2015 A hybrid roll-to-roll AFM set-up for high throughput tip-based nano-machining *Manuf. Lett.* **6** 10–3
[39] Yan Y D, He Y, Geng Y Q, Hu Z J and Li H 2016 Review on AFM tip-based mechanical nanomachining: the influence of the input machining parameters on the outcomes *Curr. Nanosci.* **12** 666–75
[40] Chen Y L, Cai Y D, Tohyama K, Shimizu Y, Ito S and Gao W 2017 Auto-tracking single point diamond cutting on non-planar brittle material substrates by a high-rigidity force controlled fast tool servo *Precis. Eng.* **49** 253–61